Longitudinal Disorder Of Superconducting Vortices

A thesis submitted in partial fulfillment of the requirement
for the degree of Bachelor of Science in
Physics from the College of William and Mary in Virginia,

by

William H. Ashton III

Advisor: Dr. Kossler

Williamsburg, Virginia
May 2001

Abstract

A continued study of the longitudinal disorder of superconducting vortices in BSCCO ($Bi_2Sr_2CaCu_2O_8$) started by Christopher Fetsch and Ken Baranowski is presented. The nature of the temperature dependence of disorder of superconducting vortices is explored. Data using μSR spectroscopy on BSCCO were analyzed using back-to-back exponential field distributions. These results were compared to field distributions arising from disordered pancake vortices. Brief discussions of superconductivity and muon spin rotation techniques are included. Results of analysis are presented as well as future steps for analyzing results. The experimental temperature dependence for $25K < T < T_c$ of a field distribution asymmetry parameter is opposite to that expected from the disordered pancake model. The field distribution in this temperature range has a longer low field tail than on the high field side.

Acknowledgments

I would first like to thank Dr. Kossler for guiding me through this research project. His guidance and instruction over the past year has been invaluable.

I would also like to thank Dr. Griffioen for keeping everything in line and on schedule.

Contents

1 Introduction

1.1 Overview

The main purpose of this research project is to study superconductors and determine if there is a connection between the temperature of the superconducting material and the disorder present in the material. This paper will outline the results obtained from the experiments. I will begin by giving a brief introduction to superconductors. I will then move on to describe the equations used and the calculations made. I will finish up by discussing the results and what they imply.

1.2 Superconductivity

Superconductors are materials that, below a certain temperature, T_c, pass electric current at zero resistance. Superconductors are diamagnetic. As a consequence, a superconductor will expel magnetic flux lines.

There are two important parameters associated with all superconductors, λ, the penetration depth, and ξ, the coherence length. The variable ξ is a fundamental length scale over which local fields within a material have an appreciable effect on the current at a nearby point, or alternatively the length scale over which the superconducting electron density varies. Superconductor type is determined by $k = \lambda/\xi$, the Ginzburg Landau parameter. A Type I superconductor has $k < 1/\sqrt{2}$, while a Type II superconductor has $k > 1/\sqrt{2}$ [1].

Type I superconductors repel a magnetic field to a value H_c. For low strength fields, Type I superconductors completely repel the magnetic field. Then, at some critical field strength, the superconductor suddenly lets all of the magnetic field through. So, a magnetic field is completely repelled, up to a critical point, where it is completely allowed.

Type II superconductors are a little different. Like a Type I, a Type II supercon-

ductor will completely repel a magnetic field up to a certain point, H_{c1}. However, at this point, instead of sharply transition to a repelled state, it enters a mixed state. This mixed state exists up to a certain field strength, H_{c2}, where the superconductor then allows all magnetic field lines, just like the Type I above. It is this mixed state that we are interested in here. The particular Type II superconductor material we are interested in here is BSCCO ($Bi_2Sr_2CaCu_2O_8$). BSCCO has a very high Tc (about 92 K) which makes it a superconductor at liquid nitrogen temperatures.

When in the mixed state, the allowed magnetic field lines form vortices. These vortices arrange themselves in an ordered triangle lattice, also called a Flux Line Lattice (FLL), see Figure 1. These vortices can be treated as either continuous tubes, like spaghetti, or as stacks of vortex slices, like pancakes.

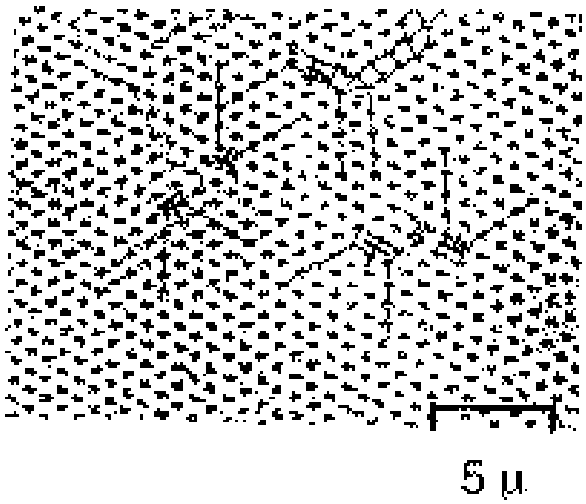

Figure 1: Flux lines in well annealed Pb (4% In) alloy. [2]

1.3 μSR

The technique that was used in this case was Muon Spin Rotation (μSR). This technique is used to measure magnetic field. Muons are unstable particles which decay with a mean lifetime of about 2 μs. A muon decays in what is known as a three-body

decay.

$$\mu^+ \rightarrow e^+ + \nu_e + \bar{\nu}_\mu \tag{1}$$

or

$$\mu^- \rightarrow e^- + \bar{\nu}_e + \nu_\mu \tag{2}$$

What we are interested in here are the emerging positrons from the μ^+ decay . These are collected by detectors surrounding the sample. By analyzing which detectors the positrons trigger, the magnetic field can be measured.

The muons themselves are obtained from pions. Pions decay weakly according to

$$\pi^+ \rightarrow \mu^+ + \nu_\mu \tag{3}$$

or

$$\pi^- \rightarrow \mu^- + \bar{\nu}_\mu \tag{4}$$

with an average lifetime of $\tau_\pi = 26$ ns. Both of these decays are shown in Figure 2.

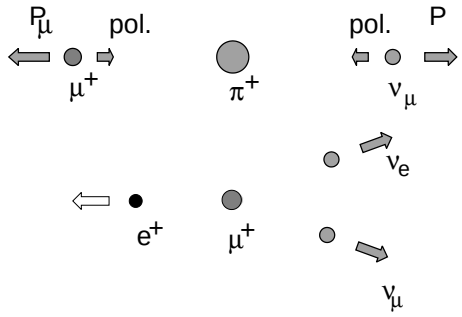

Figure 2: Illustration of decay of pion to muon, then muon to positron

The way these spin polarized muon beams were produced was by making use of very low energy pions which have already stopped near the surface of the primary production target. In the case of negative pions, these would be captured almost immediately by the target nuclei and the free decay into muons and neutrinos would not be observed. However, positive pions, now at rest, which remain somewhere

between the target constituents, decay according to Eq. 3. Positive muons emerging from the π^+ decay with the pions at rest are 100% spin polarised with respect to their momentum or flight path. Since the spin of the pion is zero, the conservation of angular momentum requires that the μ^+ and the ν_μ must also together add up to zero angular momentum. The helicity of the ν_μ, $< \sigma \cdot p >$ is fixed at $H = -1$, and thus the spin of the ν_μ is fixed anti-parallel to its momentum. Since the spin of the ν_μ is anti-parallel to its momentum, so must the spin of the μ^+ be anti-parallel to its momentum. Most of the polarization is retained while leaving the production target. Electron scattering is mostly forward and there are few larger angle nuclear scattering events. If muons of approximately a certain momentum direction are collected into a beam, this beam will show an almost 100% spin polarisation [3].

Using μSR, we can measure the internal magnetic field distribution in the mixed state of the Type II superconductor with a resolution of about 0.1 mT, which is on the order of the magnetic fields caused by nuclear dipoles. The advantages of μSR are that since the muon is a spin-1/2 particle with no quadrupole moment, there are no splittings due to quadrupolar interactions. The second advantage is that the electric charge of the muon is +1, so the Knight-shift [4] contribution is greatly reduced compared to other techniques. This makes the spectrum for μSR easier to relate to the distribution of local magnetic fields in the sample [5].

The actual data collection was done at the TRIUMF accelerator, on the campus of the University of British Columbia. The muons in this experiment were spin-rotated to have spin up ($\hat{y}$). The muons were passed, one at a time, into a region in which a superconducting magnet produced a field parallel to the muon momentum ($\hat{z}$). This caused the muons to precess (in the xy plane). The muons would then decay as described above. The resulting positrons were then collected by detectors. Figures 3 and 4 are illustrations of the experimental setups, somewhat different from the one we used, but are illustrative of μSR apparatuses used to collect data. The detectors

are labeled F, B, U, and D (Front, Back, Up, Down) in Figure 3. Figure 4 only shows the front and back detectors, however, you can clearly see the Helmholtz coils which produce the magnetic field in the region. The muon beam enters from the right in Figure 3 and from the left in Figure 4. For more information on the setup for the data collection, see ref. [6].

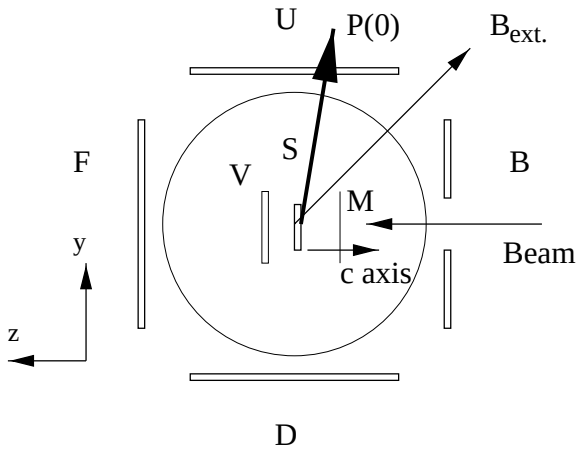

Figure 3: Illustration of experimental setup for data collection

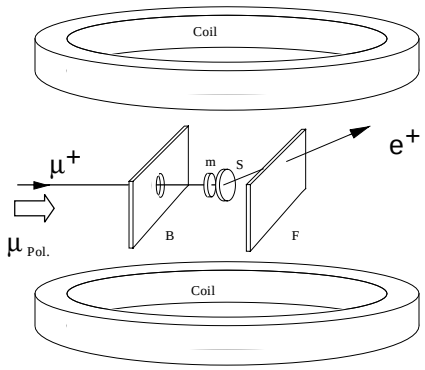

Figure 4: A second illustration of experimental setup for data collection

1.4 London Equations

The London Theory is a phenomenological theory [7]. The London equation is derived by minimizing the free energy associated with the kinetic energy of the superconducting electrons and the magnetic field energy. The London equation itself is:

$$h - \lambda_L^2 \nabla^2 h = \phi_0 \delta_2(r) \tag{5}$$

This equation may be solved for one vortex, yielding:

$$h_v(r) = \frac{\phi_0}{2\pi\lambda^2} K_0(\frac{r}{\lambda}) \tag{6}$$

where ϕ_0 is the flux quantum and K_0 is the zeroth order Bessel function of imaginary argument.

To calculate the fields for longitudinally disordered vortices we first calculate the fields for a regular array, subtract nearby individual ordered vortices, and then add back in the fields from nearby disordered pancakes, which are described below.

The fields for a regular lattice are obtained by using the solution to the London equation in reciprocal lattice space:

$$h(G) = B/(1 + \lambda_L^2 G^2) \tag{7}$$

The real space fields are:

$$h(r) = \sum_i h(G) e^{iG \cdot r} \tag{8}$$

and

$$G_j \cdot r_i = n2\pi \tag{9}$$

The nearby regular vortex fields, which will be subtracted, are obtained from

$$h(r) = \sum_i h_v(r - r_i) \tag{10}$$

The pancake fields which are then added back in are obtained as described below.

1.5 Pancake Vortices

The final part of the calculation involves the pancake vortices. The model for pancake vortices[8, 9] comes from picturing the sample in alternating layers (along z) of superconducting material and insulating material. A pancake vortex is a vortex originating in a given layer (z = 0). The z component of the magnetic field for such a vortex described in spherical coordinates is:

$$b_z(r,z) = \phi_0/(2\pi\Lambda r)e^{-r/\lambda} \tag{11}$$

Now we get that

$$b(r) = \sum b_z(r - r_{i,j,k}, z - z_{i,j,k}) \tag{12}$$

Where k is the plane of the vortex, and i and j are the location within that plane. By combining these three calculations, we can get an accurate picture of the magnetic fields. The other important part of modeling using the pancake vortices, is that it brings in disorder. Each layer of superconducting material has a 2D vortex array at a certain point. The next layer of superconducting material will also have a vortex array, but it can wander some from the first. The next wanders some from the one before it, and so forth, until eventually the vortex exits out the other side at a completely random spot, that has nothing to do with where it started. John Clem [9]gives a good argument for why we should expect to find disorder at higher temperatures. He shows that the energies required to shift one pancake vortex out of alignment (and thus create disorder in the entire stack) is so small, that as T goes to T_c, the thermal energy k_BT can strongly disalign a vortex, and thus disrupt the entire stack [9]. What we are going to try to do with this research is to quantify the disorder as a function of temperature.

2 Calculations

2.1 London Calculations

The original set of calculations on actual data was done using FORTRAN programs developed by Christopher Fetsch [10]. These programs (hxpy.f , hspag.f, and hsum.f) calculated the total magnetic field. The code hpxy.f calculates the field from the pancakes nearest the origin. The program hspag.f calculates the near direct lattice fields. The routine hsum.f calculates the reciprocal lattice results. These three programs were used repeatedly in other programs that we created during the various stages of this project.

The first step was to analyze data with the London equations (regular array with density variations). When this was done, we found that we could fit data for $YBa_2Cu_3O_7$ (Figure 5) pretty well for the first couple of microseconds. To test the accuracy of this fitting function, we created a fake data generator. This program generates fake data based on the London equation (Figure 6), so it should be fairly trivial for the fitting function to match it. The fake data generator was then modified to include statistical variation to make it more random. This fake data strongly resembled the real data we had (Figure 7). After getting this program to work, the next step was to fit these fake data with the fitting function based on the London equations.

2.2 Pancake Calculations and Fake Data

Having successfully fit the fake data with the London equation fitting function, we moved on to the next phase, using Equations 11 and 12 to fit the data. The first step in this process was to write a program that would create fake pancake data. The ultimate result of this work was a program called longdis. Longdis would read in the parameters, `B` (the external magnetic field), `xlab` (the penetration depth), `sc` (the

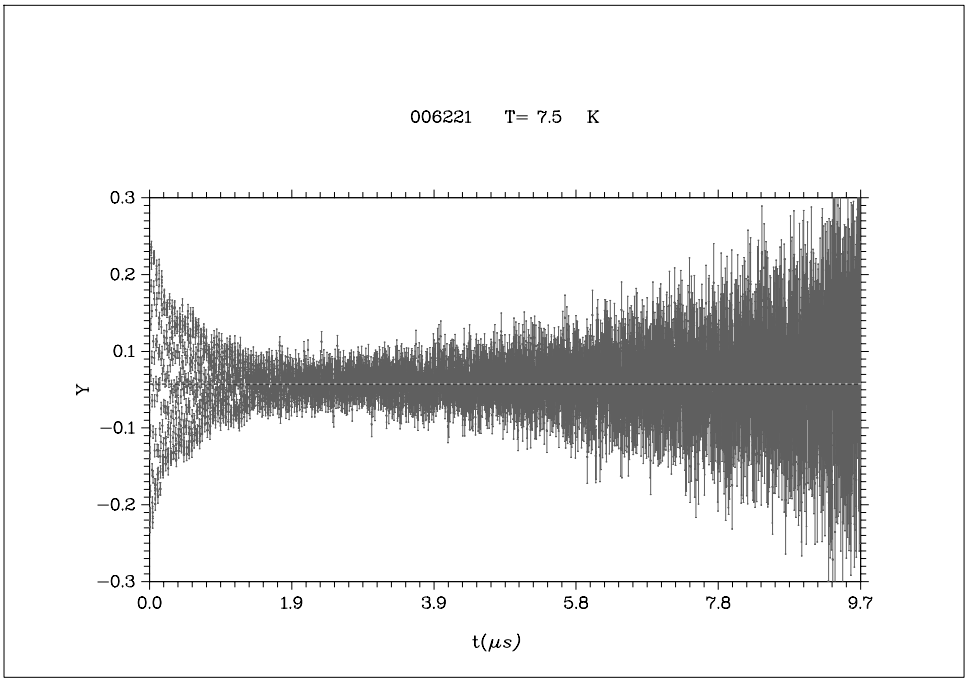

Figure 5: Plot of real data, run 006221, collected at TRIUMF

scaling factor, default 0 the first time through), `nsh` (the number of sheets up and down that are calculated), `npanxy` (the number of vortices in the x and y directions that are calculated), and `nave` (the number of times the calculation is performed and averaged). Longdis takes this information and first creates an ordered (no wandering cores) field array. It will then ask again for `sc` and `nave`. `Sc` (the scaling factor) is our measure of disorder. 0 `sc` is equivalent to no disorder. From this point, the program will calculate the modified field array with the desired disorder, then calculate B-average and σ^2 -B. The other important output is the file that shows the distribution of the internal B-field.

With this program, we calculated the internal B-fields for the cases where the applied B-field was 70, 1000, and 10000 Gauss, with varying disorder. We then created a program baver.f which would take in the output files from longdis.f and calculate B average, (B - $B_{average}$)^2, (B - $B_{average}$)^3 , and α, where

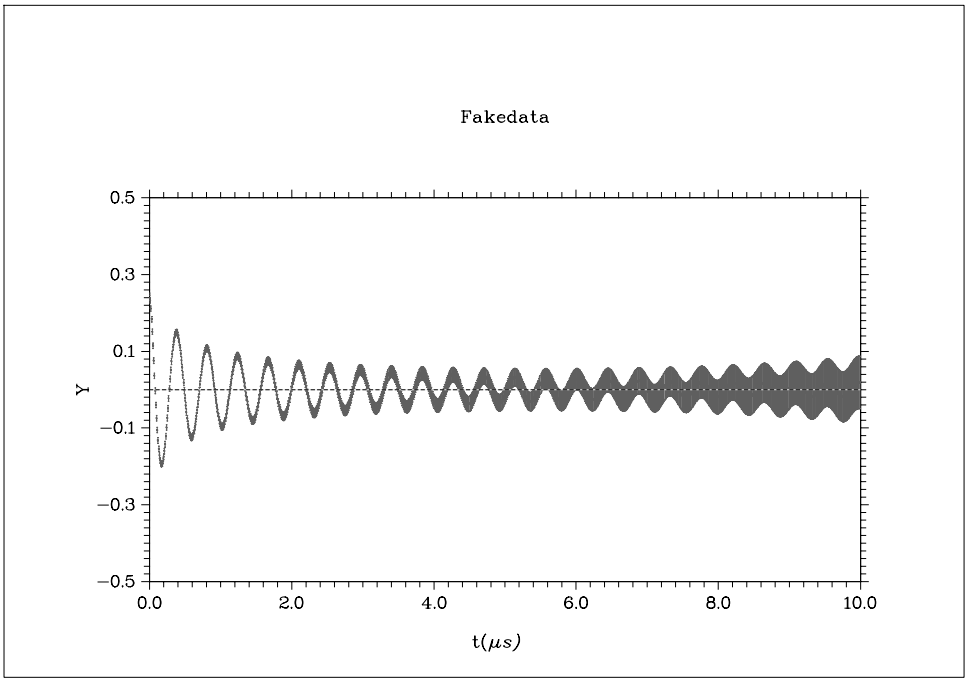

Figure 6: Plot of fake data created by fake data generator

$$\alpha = \frac{((b - b_{average})^3)^{1/3}}{\sqrt{(b - b_{average})^2}} \tag{13}$$

After calculating these results, we created a program to smear the data so that it would look more realistic. The program smearing.f read in the longdis.f output files and smeared them according to the prescription:

$$\frac{dn}{db_{sm}}(b) = \sum_{b'} \exp\left(\frac{-(b - b')^2}{2\sigma^2}\right) \frac{dn}{db}(b') \tag{14}$$

From there, we ran baver.f on the smeared results. With the smeared files we could then put together plots of alpha, B-average, (B - $B_{average}$)^2, and (B - $B_{average}$)^3, all vs. sc.

We were now ready to put together a fitting function for real data. We chose a back to back exponential frequency distribution. Thus:

$$Y(t) = \epsilon \cdot \sum \exp\left(-\frac{\mid \omega - \omega_0 \mid}{\omega_{L\,or\,R}}\right) \cos(\omega t + \phi)/N \tag{15}$$

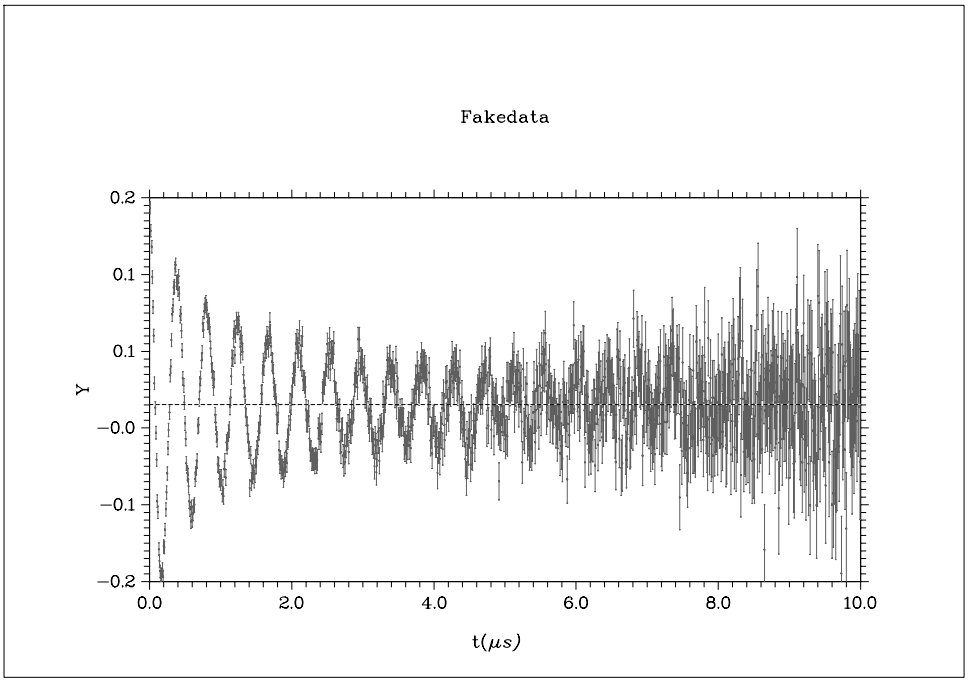

Figure 7: Plot of fake data created with statistical variation

where N is so as to normalize the sum of the exponential, one uses ω_L or ω_R depending on whether ω is less than ω_0, ϕ is a phase shift, and ϵ is the original amplitude. We can define $\omega m = (\omega_L + \omega_R)/2$ and $d\omega = \omega_L - \omega_R$ the change in frequency, ω_0 as the original frequency, and ϕ as the phase shift. We cycled real data (T = 98K to 2.5K) through this fitting function. The next program that was created was alphac.f. Alphac.f read in ωm, dω, and ω_0. It would then calculate ω1, ωs, ωc, and α. By plotting α vs T, we can get an idea of the temperature dependence of the disorder.

3 Results

One of the most interesting piece of data that we got out of all of our calculations was the plot of dω vs T(K), Figure 8. What we see in this plot is a long right hand tail at low temperatures, with a left hand tail appearing at high temperatures. What we expected to see was just the long right handed tail. This would correspond to a graph

which started where this one does at low T, then grew like an inverse exponential curve towards zero.

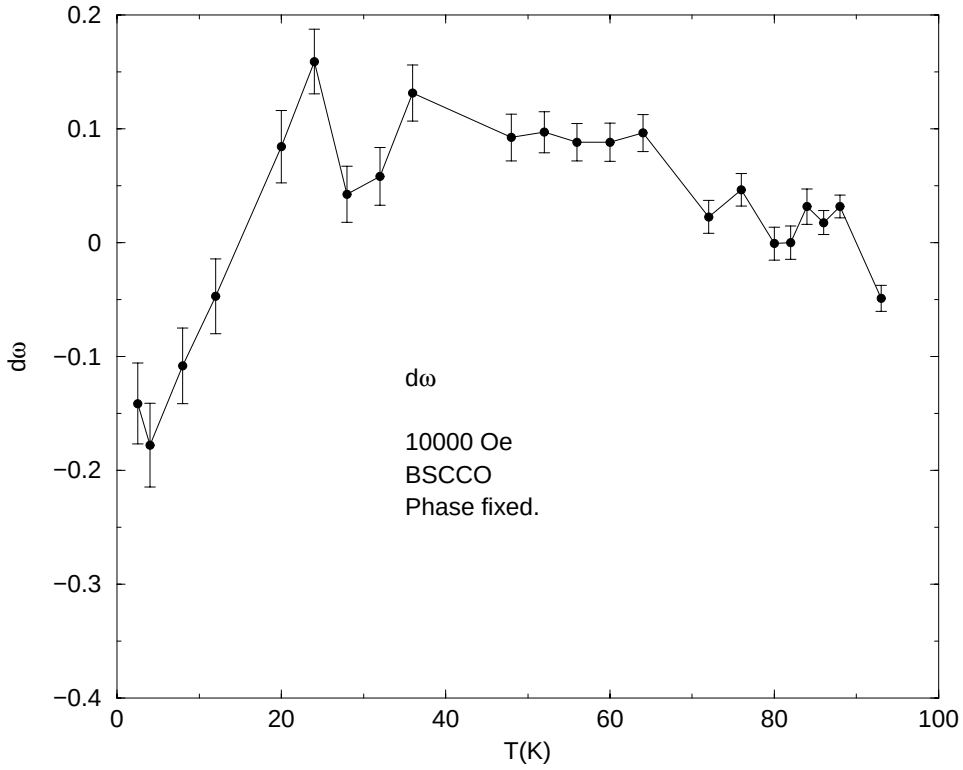

Figure 8: Plot of dω vs. T(K)

The other interesting information that we pulled out of our back-to-back exponential fits is the plot of ωm vs. T(K), Figure 9. What makes this Figure so interesting is that it is not at all what we expected to see. For a regular vortex lattice $\frac{1}{\lambda^2}$ is proportional to $\sqrt{< (b - \bar{b}^2) >}$ [11, 12] which in turn is proportional to ωm. However for BCS superconductors and even for YBCO, $\frac{\lambda(0)^2}{\lambda(T)^2}$ curves like those of Figure 10 are obtained. Note that ωm(T) is nearly linear.

The rest of our results were fairly normal. Figure 11 shows plots of the B field distribution with five different values for the disorder parameter, sc. We can see the long tail to the right, as predicted by Figure 8, even though these are London-equation-based fits. However, there is a fairly obvious lack of a tail on the left hand

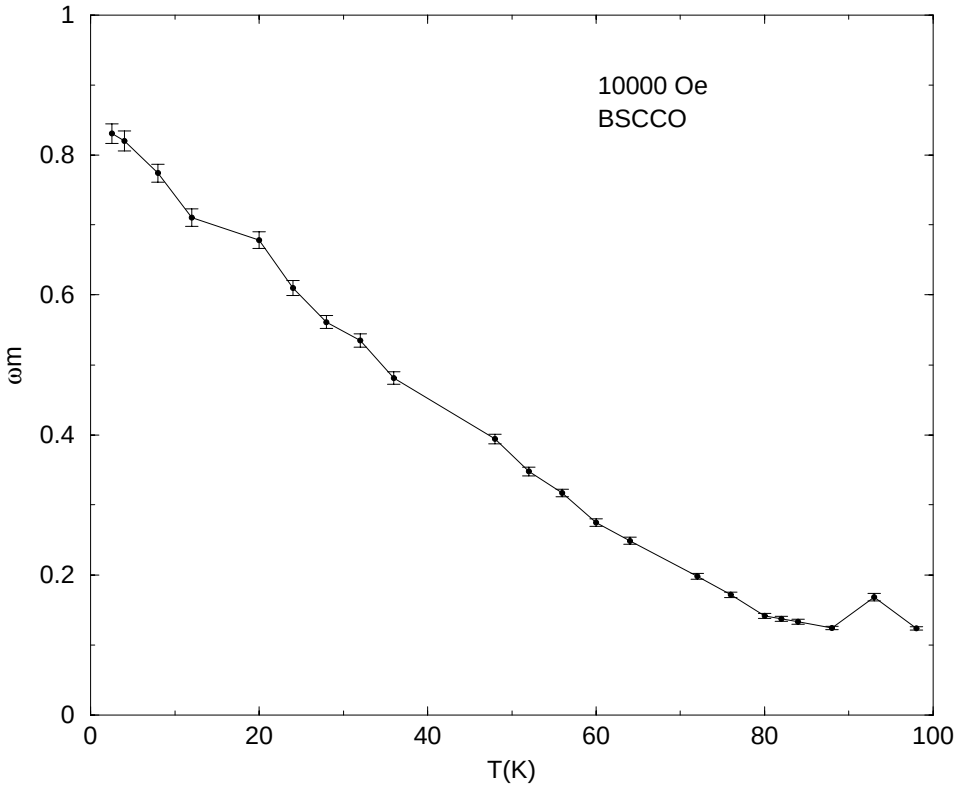

Figure 9: Plot of ωm vs. T(K)

side, even though the existence of a small one was predicted in Figure 8. Note, also, the shifting of line shape as sc goes from 0 to 0.6. The sc = 0 line is very asymmetric, with a long tail off to the right. This corresponds to a very regular FLL. The peak is the center of the vortex, and the tail is the drop-off around the peak towards the saddle points between the shown vortex and the surrounding vortices. As the disorder parameter increases, the line shape becomes more like a spike. The peak becomes taller and more symmetric as the tail gets chopped off. This is also to be expected. As the disorder increases, the location of the vortices becomes more random. So, instead of having very regularly spaces areas of magnetic field, they are spread out all over the sample, thus making the field distribution more uniform.

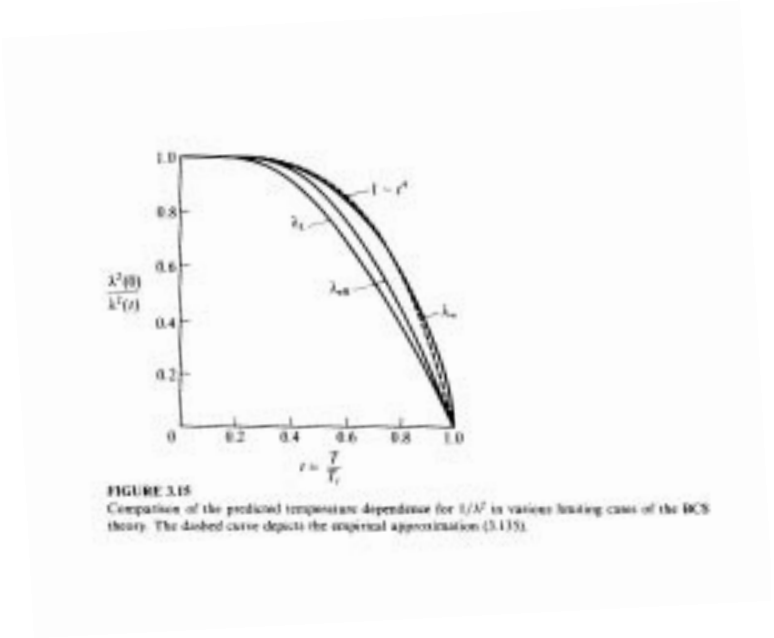

FIGURE 3.15
Comparison of the predicted temperature dependence for $1/\lambda^2$ in various limiting cases of the BCS theory. The dashed curve depicts the empirical approximation (3.135).

Figure 10: Predicted temperature dependence of $1/\lambda^2$ in various limiting cases [13]

4 Conclusions

There were some things that we did not test due to time restrictions. For example, we were unable to shed light on the puzzling results from Figures 8 and 9. The next step in that case would have been for us to go back to our fake data generator and generate a set of fake data with sc = 0, and a set of fake data with sc = 0.1, while varying λ. Since λ is linearly proportional to T, we could then plot λ vs. dω and see if we get the results of Fig 8.

We did not reach our overall goal of quantifying the dependence of disorder on temperature. We did, however, find some interesting results that definitely warrant further investigation.

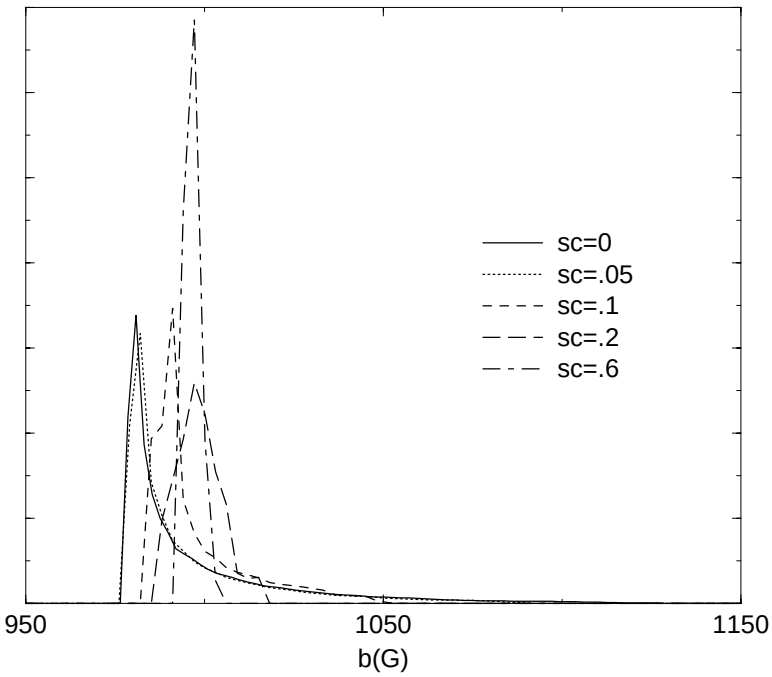

Figure 11: This is a series of plots of the B field probability distribution with varying disorder parameters

References

[1] A. J. Greer and W. J. Kossler. *Low Magnetic Fields in Anisotropic Superconductors*, volume **m30** of *Lecture Notes in Physics*. Springer-Verlag, Berlin (1995).

[2] H. Traüble and U. Essmann. "Flux-line arrangement in superconductors as revealed by direct observation." *J. Appl. Phys.*, **39**(1968) 4052.

[3] A. Schenck. *Muon Spin Rotation Spectroscopy*. Adam Hilger Ltd., London (1985).

[4] N. W. Ashcroft and N. D. Mermin. *Solid State Physics*. W. B. Saunders, New York (1976).

[5] Jeff E. Sonier, Jess H. Brewer, and Robert F. Kiefl. "μSR studies of the vortex state in type-II superconductors." *Reviews of Modern Physics*, **72**(2000) 769.

[6] K.L. Baranowski and W.J. Kossler. "Longitudinal Disorder of Superconducting Vortices." REU research, College of William and Mary, 2000.

[7] F. London and H. London. "Electromagnetic Equations of the Superconductor." *Proc. Roy. Soc. (London) A*, **149**(1935) 71.

[8] John R. Clem. "Properties of 2D Pancakes." *Bull. Am. Phys. Soc.*, **42**(1997) 701.

[9] John R. Clem. "Two-dimensional vortices in a stack of thin superconducting films: A model for high-temperature superconducting multilayers." *Phys. Rev. B*, **43**(1991) 7837.

[10] Christopher Fetsch. "Longitudinal disorder of superconducting pancake vortex arrays." Senior Thesis, College of William and Mary, May 2000.

[11] E. H. Brandt. "Flux distribution and penetration depth measured by muon spin rotation in high-T_c superconductors." *Phys. Rev B*, **37**(1988) 2349.

[12] W. Barford and J. M. F. Gunn. "A theoretical interpretation of μSR experiments to measure the London penetration depth in anisotropic type II superconductors." *Physica C*, **156**(1988) 515.

[13] M. Tinkham. *Introduction to Superconductivity*. McGraw-Hill, New York (1996).